PHYSICAL REVIEW C VOLUME 51, NUMBER 1 JANUARY 1995

Microscopic abrasion-ablation approximation to projectile fragmentation

B. V. Carlson*
National Superconducting Cyclotron Laboratory, Michigan State University, East Lansing, Michigan 48824
(Received 29 June 1994)

This microscopic abrasion-ablation model approximates primary fragment cross sections using the Glauber interaction probabilities of the individual nucleon orbitals. It estimates the excitation energy distribution of the primary fragments using the density of hole states left by the abraded nucleons. The secondary (observable) cross sections are obtained by taking into account the statistical decay of each primary fragment over its entire range of excitation energy. The agreement with experimental data is good for light projectiles but deteriorates with increasing mass of the projectile, due to the increasing importance of secondary collisions of the abraded nucleons with the rest of the projectile.

PACS number(s): 25.70.Mn

I. INTRODUCTION

Fragment emission has been recognized as a common feature of heavy-ion reactions at intermediate and higher energies for many years now [1–6]. Its importance and subtleties are confirmed by the fact that it continues to be the subject of experimental [7–12] and theoretical [13–17] study. The process has also won a great deal of current interest as a means for producing secondary beams of exotic nuclei [18].

One of the first models to attempt a description of heavy-ion fragmentation was the abrasion-ablation one of Bowman, Swiatecki, and Tsang [2]. In the model's abrasion stage, the nucleons in the overlap volume of two energetic heavy ions are scraped off (abraded) as the ions pass each other. In the subsequent ablation stage, the excited projectile and target fragments decay by emitting particles. Bowman, Swiatecki, and Tsang estimated the excitation energy of each fragment as the difference in the surface energy of the abraded fragment and that of a sphere of equal volume. Although the model succeeds in describing the overall characteristics of the data, it systematically overestimates the cross sections of fragments from which few nucleons had been abraded. Final-state interactions, introduced in the model's abrasion stage by Hüfner, Schäfer, and Schürmann [3] and also Oliveira, Donangelo, and Rasmussen [6], succeed in providing the extra energy needed for the discrepant nuclei to decay.

However, final-state interactions muddy the model's clean division of the nucleons into participants and spectators of the reaction. Once the abraded nucleons are taken into consideration when calculating a fragment's excitation energy, it is difficult to argue that they would not influence its charge and mass by abrading other nucleons. Thus, instead of completing the abrasion-ablation picture of fragmentation, the introduction of a final-state interaction makes its inadequacies apparent.

Although over 20 years have gone by since the abrasion-ablation model was proposed, work on projectile fragmentation continues. In the time that has passed, the great increase in computing power and reduction in its cost have made the dynamical simulation of heavy-ion reactions feasible. Among the available models are the cascade [19] and Boltzmann-Uehling-Uhlenbeck (BUU) [20] ones and the various versions of molecular dynamics [21–23]. One hopes, by using one of these, to obtain a more accurate description of the abrasion of nucleons and deposition of energy occurring in the initial stage of the collision. Each of these models has individual advantages and drawbacks, making them more or less suitable for the description of fragmentation reactions. But, because of their complexity, all are much more time consuming than a geometric or Glauber abrasion calculation.

Two recent works have used a revised abrasion-ablation model consistent with the spectator-participant picture in one more attempt to obtain a simple description of the observed experimental fragmentation yields [14,16]. They approximate the primary fragment excitation energy as that of the holes left by the abraded nucleons. The resulting excitation energy is, on the average, two to three times larger than that obtained in the original abrasion-ablation model. The agreement of these models with the light-projectile data is surprisingly good, given that they do not take into account the final-state interactions found to be important in earlier calculations. However, after looking more closely, one finds that final-state interactions are still needed to obtain agreement with the experimental data, although to a lesser degree for light projectiles than for heavy ones.

This work attempts to provide a microscopic foundation for the revised abrasion-ablation models of Refs. [14,16]. It begins with a careful derivation of the expressions for the microscopic abrasion cross sections and for the secondary yields after ablation. Calculations with the model are then compared to experimental data

*Permanent address: Divisão de Física Teórica, Instituto de Estudos Avançados, Centro Técnico Aeroespacial, 12231 São José dos Campos SP, BRAZIL.

and to dynamical simulations using the BUU approach. The comparison with BUU simulations sheds light on the manner in which the microscopic abrasion calculation might be later extended to include more of the physics of the fragmentation process.

II. THEORETICAL DEVELOPMENT

In this section, expressions for the microscopic abrasion cross sections are derived. In the first part, "exact" expressions for the abrasion cross sections are obtained. In the second, approximations are made that reduce these to a calculable form. Finally, the calculation of secondary ablation yields is discussed.

A. Derivation of Glauber amplitudes and cross sections

Let us begin, as do Hüfner, Schäfer, and Schürmann [3], with the Glauber approximation to the amplitude for the scattering of a projectile (P) by a target nucleus (T) [24],

$$F_{O_P O_T \to M_P M_T}(\mathbf{q}) = \frac{k}{2\pi i}\int d^2b\, e^{i\mathbf{q}\cdot\mathbf{b}}\left\langle M_P M_T\left|\prod_{j\in P, l\in T} e^{i\chi_{jl}} - 1\right|O_P O_T\right\rangle. \tag{1}$$

The two ions, initially in their respective ground states, $|O_P\rangle$ and $|O_T\rangle$, are excited to states $|M_P\rangle$ and $|M_T\rangle$, respectively. We will assume that the fast nucleons in the projectile can be distinguished from the slow ones in the target and thus neglect antisymmetrization between the ions.

The transition operator contains the phase shift "functions," $\chi_{jl} = \chi_{jl}(\mathbf{s}_j + \mathbf{b} - \mathbf{s}_l)$ for the scattering of nucleon j of the projectile by nucleon l of the target. If we take the projectile to move in the z direction, we can decompose the position vector $\mathbf{x}_j$ of particle j (with respect to the projectile center of mass) into its z component and a component $\mathbf{s}_j$ in the impact parameter plane, $\mathbf{x}_j = (\mathbf{s}_j, z_j)$. The target coordinate $\mathbf{x}_l$ can be decomposed similarly with respect to the target center of mass, $\mathbf{x}_l = (\mathbf{s}_l, z_l)$. The impact parameter $\mathbf{b}$ denotes the relative position of the two centers of mass in the plane perpendicular to the z direction.

Although we will not assume that the nucleons only scatter elastically, we will assume that the basis is large enough to ensure that the $e^{i\chi_{jl}}$ are unitary. (χ_{jl} could be a matrix including such processes as $N + N \to N + \Delta, \Delta + \Delta$, etc. The basis would then have to include these channels as well.)

Returning to the expression for the scattering amplitude, we can write the angular distribution in its terms as

$$\frac{d\sigma}{d\Omega}^{O\to M_P M_T}(\mathbf{q}) = |F_{O\to M_P M_T}(\mathbf{q})|^2, \tag{2}$$

where we have abbreviated the initial state as $O = O_P O_T$.

As we will not observe the final states of the target, we can sum over them and use closure to eliminate M_T from the expression. We have

$$\begin{aligned}\frac{d\sigma}{d\Omega}^{O\to M_P}(\mathbf{q}) &= \sum_{M_T}|F_{O\to M_P M_T}(\mathbf{q})|^2 \\ &= \frac{k^2}{(2\pi)^2}\int d^2b\, d^2b'\, e^{i\mathbf{q}\cdot(\mathbf{b}-\mathbf{b}')}\left\langle O_T\left|\left\langle O_P\left|\prod_{j,l} e^{-i\chi^\dagger_{jl}(\mathbf{b}')} - 1\right|M_P\right\rangle\left\langle M_P\left|\prod_{j,l} e^{i\chi_{jl}(\mathbf{b})} - 1\right|O_P\right\rangle\right|O_T\right\rangle. \end{aligned}\tag{3}$$

To obtain the corresponding cross section, we integrate this expression over angle. We have

$$\begin{aligned}\sigma_{O\to M_P} &\approx \frac{1}{k^2}\int d^2q \frac{d\sigma}{d\Omega}^{O\to M_P} \\ &= \int d^2b\, \langle O_T|X_{O_P\to M_P}(\mathbf{b})|O_T\rangle, \end{aligned}\tag{4}$$

where

$$X_{O_P\to M_P}(\mathbf{b}) = \left\langle O_P\left|\prod_{j,l} e^{-i\chi^\dagger_{jl}(\mathbf{b})} - 1\right|M_P\right\rangle\left\langle M_P\left|\prod_{j,l} e^{i\chi_{jl}(\mathbf{b})} - 1\right|O_P\right\rangle. \tag{5}$$

It is this last expression that we will now try to simplify. To do this, we must first characterize the initial and final states.

We will assume that both the initial and final states can be expressed as antisymmetrized products of single-particle states. We denote the set of initially occupied states by $\mathcal{O}_0$ and take their number to be A_0. We assume that the final states of interest will be those describing the

occupancy (or vacancy) of a set of single-particle states that we denote by $\mathcal{M}_0$. The set of final states, $\mathcal{M}_0$, will contain the set of initally occupied states, $\mathcal{O}_0$, but need not be restricted to them.

A final state will be characterized by the subset of $\mathcal{M}_0$ of occupied single-particle states, which we will denote by occ, and by the single-particle states, μ_i, not contained in $\mathcal{M}_0$, that the remaining nucleons occupy. The final number of occupied states in $\mathcal{M}_0$, $A_{\rm occ}$, cannot exceed the initial number of nucleons, A_0: $A_0 \geq A_{\rm occ}$.

We write the antisymmetrized initial state as

$$\langle \mathbf{x}_1, \ldots, \mathbf{x}_{A_0} | O_P \rangle = \frac{1}{\sqrt{A_0!}} \sum_p (-1)^p \prod_{j=1}^{A_0} \langle x_{p(j)} | o_j \rangle, \quad (6)$$

where we denote by p each of the possible $A_0!$ permutations of the indices. We can write the final state in a similar manner as

$$\langle \mathbf{x}_1, \ldots, \mathbf{x}_{A_0} | M_P \rangle = \frac{1}{\sqrt{A_0!}} \sum_p (-1)^p \prod_{j=1}^{A_{\rm occ}} \langle x_{p(j)} | m_j \rangle \prod_{j=A_{\rm occ}+1}^{A_0} \langle x_{p(j)} | \mu_j \rangle, \quad (7)$$

where we have denoted the set of states occ by $\{m_1, \ldots, m_{A_{\rm occ}}\}$.

To simplify the notation slightly, we follow Ref. [3] in defining for each nucleon in the projectile,

$$Q(\mathbf{x}_j) = \prod_{l \in T} e^{i\chi_{jl}(\mathbf{b})} . \quad (8)$$

We then write the matrix element as (we neglect the 1 for the moment)

$$\left\langle M_P \middle| \prod_j Q(\mathbf{x}_j) \middle| O_P \right\rangle = \frac{1}{A_0!} \int \prod_{j=1}^{A_0} d^3x_i \sum_{p,p'} (-1)^{p+p'} \prod_{j=1}^{A_{\rm occ}} \langle m_j | \mathbf{x}_{p'(j)} \rangle \prod_{j=A_{\rm occ}+1}^{A_0} \langle \mu_j | \mathbf{x}_{p'(j)} \rangle \prod_{j=1}^{A_0} Q(\mathbf{x}_j) \prod_{j=1}^{A_0} \langle \mathbf{x}_{p(j)} | o_j \rangle. \quad (9)$$

Since the product $\prod_j Q(\mathbf{x}_j)$ is symmetric in the coordinates, it is invariant under permutations. We can thus remove the permutation p' from the final-state coordinates, pass it through the product, and apply it to the initial coordinates. We can then go one step further and apply the permutations to the initial-state index rather than the coordinate one. (In practice, this is a change of variables, but they are dummy variables.) Finally, we rearrange the matrix element as

$$\left\langle M_P \middle| \prod_j Q(\mathbf{x}_j) \middle| O_P \right\rangle = \frac{1}{A_0!} \sum_{p,p'} (-1)^{p+p'} \prod_{j=1}^{A_{\rm occ}} \int d^3x_j \langle m_j | \mathbf{x}_j \rangle Q(\mathbf{x}_j) \langle \mathbf{x}_j | o_{pp'(j)} \rangle$$

$$\times \prod_{j=A_{\rm occ}+1}^{A_0} \int d^3x_j \langle \mu_j | \mathbf{x}_j \rangle Q(\mathbf{x}_j) \langle \mathbf{x}_j | o_{pp'(j)} \rangle. \quad (10)$$

Now we observe that the matrix element only depends on the permutation pp'. We can thus redefine the sum $\sum_{p,p'}$ as another sum $\sum_{p,q}$ with $pp' \to p$ and $p' \to q$. The sum over the permutations q is trivial and cancels the factor of $1/A_0!$, leaving us with

$$\left\langle M_P \middle| \prod_j Q(\mathbf{x}_j) \middle| O_P \right\rangle = \sum_p (-1)^p \prod_{j=1}^{A_{\rm occ}} Q_{m_j p(j)} \prod_{j=A_{\rm occ}+1}^{A_0} Q_{\mu_j p(j)}, \quad (11)$$

where we have taken the liberty to define

$$Q_{m_j\, p(j)} = \langle m_j | Q | o_{p(j)} \rangle \quad \text{and} \quad Q_{\mu_j\, p(j)} = \langle \mu_j | Q | o_{p(j)} \rangle. \quad (12)$$

In terms of these, we can write the quantity $X_{O_P \to M_P}$ of Eq. (5) as

$$X_{O_P \to M_P}(\mathbf{b}) = \sum_{p,p'} (-1)^{p+p'} \prod_{j=1}^{A_{\rm occ}} Q^\dagger_{p'(j) m_j} Q_{m_j\, p(j)} \prod_{j=A_{\rm occ}+1}^{A_0} Q^\dagger_{p'(j)\, \mu_j} Q_{\mu_j\, p(j)}. \quad (13)$$

The next step will be to eliminate the states outside of $\mathcal{M}_0$, the μ_j that we assume will not be observed. In order to do this, we make use of a general property of antisymmetrized products, which is demonstrated in Appendix A. This is that

$$\frac{1}{N!}\sum_{p,p'}(-1)^{p+p'}\prod_{j=1}^{N}\left(\sum_{k=1}^{M}Q^{\dagger}_{p'(j)k}Q_{kp(j)}\right)=\begin{cases}0, & M<N,\\ \displaystyle\sum_{\{k_1,\ldots,k_N\}}\sum_{p,p'}(-1)^{p+p'}\prod_{j=1}^{N}Q^{\dagger}_{p'(j)k_j}Q_{k_jp(j)}, & M\geq N,\end{cases}\tag{14}$$

where, on the right-hand-side expression, we mean by $\sum_{\{k_1,\ldots,k_N\}}$ the sum over all possible N element subsets of the states $k_1,k_2,\ldots,k_M$.

We use this result to simplify the sum over the unobserved μ_j states. We denote the sum over all possible combinations of the μ_j states by $\sum_{\{\mu_P\}}$. We use the equality above to rewrite this sum of products as a product of sums. We have

$$\begin{aligned}\sum_{\{\mu_P\}}X_{O_P\to M_P}(\mathbf{b})&=\sum_{\{\mu_P\}}\sum_{p,p'}(-1)^{p+p'}\prod_{j=1}^{A_{\rm occ}}Q^{\dagger}_{p'(j)\,m_j}Q_{m_jp(j)}\prod_{j=A_{\rm occ}+1}^{A_0}Q^{\dagger}_{p'(j)\,\mu_j}Q_{\mu_jp(j)}\\&=\frac{1}{(A_0-A_{\rm occ})!}\sum_{p,p'}(-1)^{p+p'}\prod_{j=1}^{A_{\rm occ}}Q^{\dagger}_{p'(j)\,m_j}Q_{m_jp(j)}\prod_{j=A_{\rm occ}+1}^{A_0}\left(\sum_{\mu\notin\mathcal{M}_0}Q^{\dagger}_{p'(j)\,\mu}Q_{\mu p(j)}\right).\end{aligned}\tag{15}$$

We can now use closure to rewrite the sum over the states μ in terms of the states in $\mathcal{M}_0$,

$$\sum_{\mu\notin\mathcal{M}_0}Q^{\dagger}_{p'(j)\,\mu}Q_{\mu p(j)}=\delta_{p'(j)\,p(j)}-\sum_{m\in\mathcal{M}_0}Q^{\dagger}_{p'(j)\,m}Q_{mp(j)}.\tag{16}$$

We then have, for $\sum_{\{\mu_P\}}X_{O_P\to M_P}$, the expression

$$\sum_{\{\mu_P\}}X_{O_P\to M_P}(\mathbf{b})=\frac{1}{(A_0-A_{\rm occ})!}\sum_{p,p'}(-1)^{p+p'}\prod_{j=1}^{A_{\rm occ}}Q^{\dagger}_{p'(j)\,m_j}Q_{m_jp(j)}\prod_{j=A_{\rm occ}+1}^{A_0}\left(\delta_{p'(j)\,p(j)}-\sum_{m\in\mathcal{M}_0}Q^{\dagger}_{p'(j)\,m}Q_{mp(j)}\right).\tag{17}$$

We can simplify this slightly by verifying that the terms in the sum, $\sum_{m\in\mathcal{M}_0}$, that are also in the set of occupied states, occ, will vanish due to the antisymmetrization. If we define the set of vacant states in $\mathcal{M}_0$, denoted by vac, as the set of states which are not in occ, we can write the result in a somewhat symmetrical form as

$$\begin{aligned}\sum_{\{\mu_P\}}X_{O_P\to M_P}(\mathbf{b})&=\frac{1}{A_{\rm occ}!(A_0-A_{\rm occ})!}\sum_{p,p'}(-1)^{p+p'}\prod_{j=1}^{A_{\rm occ}}\left(\sum_{m\in\rm occ}Q^{\dagger}_{p'(j)\,m}Q_{mp(j)}\right)\\&\times\prod_{j=A_{\rm occ}+1}^{A_0}\left(\delta_{p'(j)\,p(j)}-\sum_{m\in\rm vac}Q^{\dagger}_{p'(j)\,m}Q_{mp(j)}\right).\end{aligned}\tag{18}$$

The expression for quasielastic scattering is similar. To obtain it, we need only include the additional diagonal terms. We note that the quasielastic expression is strictly elastic only when the initial and final sets of single-particle states, $\mathcal{O}_0$ and $\mathcal{M}_0$, coincide. When $\mathcal{M}_0$ contains additional states, it contains quasielastic contributions to the scattering. These are due to reactions in which nucleons are excited to the additional states in $\mathcal{M}_0$ instead of being abraded.

B. Optical averages and other approximations

Using the Glauber approximation to the nucleus-nucleus scattering amplitude and expressing the initial and final projectile states as antisymmetric products of single-particle states, we have derived "exact" expressions for abrasion and quasielastic cross sections. We now reduce these to a calculable form by making two simplifying approximations.

We begin by averaging over the target ground state. We write the cross section as

$$\sigma_{O\to M_F}=\int d^2b\,\overline{X}_{O\to M_F}(\mathbf{b}),\tag{19}$$

where

$$\overline{X}_{O\to M_F}(\mathbf{b})=\left\langle O_T\left|\sum_{\{\mu_P\}}X_{O_P\to M_P}(\mathbf{b})\right|O_T\right\rangle.\tag{20}$$

To evaluate the latter expression, we use the coherent approximation used in Ref. [3]. We have

$$\begin{aligned}\overline{X}_{O\to M_F}(\mathbf{b})&=\frac{1}{A_{\rm occ}!(A_0-A_{\rm occ})!}\sum_{p,p'}(-1)^{p+p'}\prod_{j=1}^{A_{\rm occ}}\left(\sum_{m\in\rm occ}\overline{Q}^{\dagger}_{p'(j)\,m}\overline{Q}_{mp(j)}\right)\\&\times\prod_{j=A_{\rm occ}+1}^{A_0}\left(\delta_{p'(j)\,p(j)}-\sum_{m\in\rm vac}\overline{Q}^{\dagger}_{p'(j)\,m}\overline{Q}_{mp(j)}\right),\end{aligned}\tag{21}$$

where the average single-particle amplitudes are given by

$$\overline{Q}_{m\,p(j)} = \left\langle m \left| \overline{\prod_{l\in T} e^{i\chi_{jl}(\mathbf{b})}} \right| o_{p(j)} \right\rangle$$
$$= \int dz\, d^2s\, m^\dagger(z,\mathbf{s}) \exp\left[-i\frac{m}{\hbar^2 k}\int_{-\infty}^{\infty} dz\, U_T^{\rm opt}(z,\mathbf{b}-\mathbf{s})\right] o_{p(j)}(z,\mathbf{s})\,. \tag{22}$$

The quasielastic expression is similar in form to the abrasion ones.

Although these expressions are in principle calculable, their calculation would still be quite demanding. At each impact parameter, we would need to obtain at least $A_0(A_0+1)/2$ matrix elements, $\overline{Q}_{m\,p(j)} = (\overline{Q}^\dagger_{p(j)\,m})^*$ (more if $\mathcal{M}_0$ contains more states than those in $\mathcal{O}_0$) which would then have to be combined in antisymmetric products. To avoid this, we make yet another simplifying approximation: we neglect the matrix elements between nonidentical states. While we do indeed expect the neglected matrix elements to be small, it is not obvious that they need be negligible in comparison to the ones we keep. Yet, the approximation is an extremely convenient one. We will use it for this reason alone, keeping in mind its need of justification.

Having made this last approximation, that is,

$$\overline{Q}_{m\,p(j)} \to \overline{Q}_{p(j)}(\mathbf{b})\delta_{m\,p(j)}, \tag{23}$$

we rid ourselves of a few extra indices by redefining the surviving matrix elements as

$$\overline{Q}_j(\mathbf{b}) = \int dz\, d^2s\, o_j^\dagger(z,\mathbf{s}) \exp\left[-i\frac{m}{\hbar^2 k}\int_{-\infty}^{\infty} dz\, U_T^{\rm opt}(z,\mathbf{b}-\mathbf{s})\right] o_j(z,\mathbf{s})\,. \tag{24}$$

We note that this approximation effectively reduces the set of final single-particle states $\mathcal{M}_0$ to the set of initial ones $\mathcal{O}_0$, as it discards the matrix elements that would couple the states in $\mathcal{O}_0$ to any other states in $\mathcal{M}_0$.

With these simplifications, the permutation sums can be performed explicitly. We find

$$\overline{X}_{O\to M_F}(\mathbf{b}) = \prod_{j\in\rm occ} |\overline{Q}_j(\mathbf{b})|^2 \prod_{j\in\rm vac} \left(1-|\overline{Q}_j(\mathbf{b})|^2\right) \tag{25}$$

and

$$\overline{X}^{el} = \left| \prod_{j\in\mathcal{O}_0} \overline{Q}_j(\mathbf{b}) - 1 \right|^2 . \tag{26}$$

If we interpret the elastic $\overline{X}$ expression in terms of an S matrix,

$$S(\mathbf{b}) = \prod_{j\in\mathcal{O}_0} \overline{Q}_j(\mathbf{b}), \tag{27}$$

we can write the corrresponding transmission coefficient as

$$T(\mathbf{b}) = 1 - |S(\mathbf{b})|^2 = 1 - \prod_j |\overline{Q}_j(\mathbf{b})|^2. \tag{28}$$

The reaction cross section is then given by

$$\sigma_{\rm reac} = \int d^2b\, T(\mathbf{b}). \tag{29}$$

It can be shown that the abrasive $\overline{X}$ expressions, when summed over all configurations and all mass losses, yield the transmission coefficient,

$$\sum_{A_{\rm occ}<A_0} \sum_{\{\rm occ|A_{occ}\}} \overline{X}_{O\to M_F}(\mathbf{b}) = T(\mathbf{b}). \tag{30}$$

The abrasion cross sections thus exhaust the reaction cross section.

Similar Glauber multiple scattering expressions have been used in Refs. [13,25] to describe the elastic scattering and breakup of halo nuclei. The relationship of our expressions to those derived by Hüfner, Schäfer, and Schürmann is detailed in Appendix B.

The distinction between neutrons and proton is easily introduced by making their isospin index evident. We can write the differential contribution to the cross section of Eq. (25) as

$$\overline{X}_{O\to Z_F\,A_F}(\mathbf{b}) = \prod_{j_\nu\in\rm occ_\nu} |\overline{Q}_{j_\nu}(\mathbf{b})|^2 \prod_{j_\nu\in\rm vac_\nu} \left(1-|\overline{Q}_{j_\nu}(\mathbf{b})|^2\right) \prod_{j_\pi\in\rm occ_\pi} |\overline{Q}_{j_\pi}(\mathbf{b})|^2 \prod_{j_\pi\in\rm vac_\pi} \left(1-|\overline{Q}_{j_\pi}(\mathbf{b})|^2\right), \tag{31}$$

with all other expressions just as straightforward.

C. Primary and secondary yields

The cross sections derived above are given for a well-defined set of occupied final single-particle states. We want to transform the latter into a differential cross section that depends on the excitation energy of the final fragment. To this end, we associate a single-particle energy to each of the projectile single-particle states. Then we estimate the excitation energy in terms of the single-particle energies, ϵ_j, of the holes left by the knocked-out nucleons.

In a single-particle picture, knockout of the outermost nucleons would produce the ground state of the fragment nucleus. However, the corresponding sum over hole energies,

$$\varepsilon_0 = \sum_{j_\nu \in \mathrm{vac}_{\nu 0}} \epsilon_{j_\nu} + \sum_{j_\pi \in \mathrm{vac}_{\pi 0}} \epsilon_{j_\pi} , \tag{32}$$

would not necessarily be zero. Thus, the excitation energy, ε, must be defined relative to this "ground state" energy,

$$\varepsilon = \sum_{j_\nu \in \mathrm{vac}_\nu} \epsilon_{j_\nu} + \sum_{j_\pi \in \mathrm{vac}_\pi} \epsilon_{j_\pi} - \varepsilon_0 . \tag{33}$$

The differential primary cross section can then be written as

$$\frac{d\sigma_0}{d\varepsilon}(\varepsilon, Z_f, A_f) = \sum_{\{\mathrm{occ}_\nu, \mathrm{occ}_\pi | Z_f, A_f\}} \delta\left(\varepsilon - \sum_{j_\nu \in \mathrm{vac}_\nu} \epsilon_{j_\nu} - \sum_{j_\pi \in \mathrm{vac}_\pi} \epsilon_{j_\pi} + \varepsilon_0\right) \times \int d^2b \prod_{j_\nu \in \mathrm{occ}_\nu} |\overline{Q}_{j_\nu}(\mathbf{b})|^2 \prod_{j_\nu \in \mathrm{vac}_\nu} \left(1 - |\overline{Q}_{j_\nu}(\mathbf{b})|^2\right) \prod_{j_\pi \in \mathrm{occ}_\pi} |\overline{Q}_{j_\pi}(\mathbf{b})|^2 \prod_{j_\pi \in \mathrm{vac}_\pi} \left(1 - |\overline{Q}_{j_\pi}(\mathbf{b})|^2\right) . \tag{34}$$

Physically, the estimate of the excitation energy in terms of the hole energies corresponds to the assumption that the knocked-out nucleons leave the projectile suddenly without perturbing it while exiting. It also assumes that the remaining nucleons are true spectators, feeling no influence of the knocked-out projectile nucleons nor of the target ones. Such assumptions are consistent with the Glauber approximation to the cross sections.

The conversion from a detailed description in terms of the final occupied single-particle states to a distribution in excitation energy neglects single-particle information that could play a role in the subsequent decay of the primary fragment. In a given range of excitation energy, it is possible to have contributions to the cross section from both simple and complex particle-hole configurations. In a preequilibrium analysis, the simple configurations that concentrate the excitation energy in few particles and holes would tend to decay more rapidly than the complex ones. By lumping all configurations into an excitation-energy-dependent cross section, we have assumed that such preequilibrium effects can be neglected.

We thus assume that the decay during the ablation stage occurs by (multiple) statistical particle emission from an equilibrated primary fragment. We write the result of the evaporation calculation as the probability, $P(Z, A; \varepsilon, Z_f, A_f)$, of yielding a residue of charge Z and mass A, given a primary compound nucleus of charge Z_f, mass A_f and excitation energy ε. In terms of this quantity and the differential primary yield, $d\sigma_0(\varepsilon, Z_f, A_f)/d\varepsilon$, the secondary cross section, $\sigma(Z, A)$, can be expressed as

$$\sigma(Z, A) = \sum_{Z_f, A_f} \int d\varepsilon \, P(Z, A; \varepsilon, Z_f, A_f) \frac{d\sigma_0}{d\varepsilon}(\varepsilon, Z_f, A_f) . \tag{35}$$

It is this quantity which is to be compared with the experimental data.

III. RESULTS AND DISCUSSION

We begin this section by briefly discussing the optical potentials and the nuclear structure and statistical decay models used in the calculations, as well as the physical parameters used. We then compare calculations to experimental data for light, medium, and heavy nuclei, in turn. We close with the comparison of a Glauber abrasion calculation to a dynamical simulation performed using the BUU approach.

A. Optical potentials, wave functions, and other details

The optical potentials in the abrasion matrix elements, Eq. (24), are estimated using the impulse approximation. The real part of the forward nucleon-nucleon scattering amplitude is neglected while its imaginary part is determined by the optical theorem. The optical potential for neutrons thus reduces to

$$i\frac{2m}{\hbar^2 k} U^{\mathrm{opt}}_{T\nu}(z, \mathbf{b}) = \sigma_{pn}\rho^T_\pi(z, \mathbf{b}) + \sigma_{nn}\rho^T_\nu(z, \mathbf{b}) , \tag{36}$$

while that for protons becomes

$$i\frac{2m}{\hbar^2 k} U^{\mathrm{opt}}_{T\pi}(z, \mathbf{b}) = \sigma_{pp}\rho^T_\pi(z, \mathbf{b}) + \sigma_{pn}\rho^T_\nu(z, \mathbf{b}) . \tag{37}$$

The target proton and neutron densities, $\rho^T_\pi(z, \mathbf{b})$ and $\rho^T_\nu(z, \mathbf{b})$, are estimated using global fits to geometrical parameters obtained from elastic electron scattering data [27]. The same geometry is used for both neutrons and protons.

The neutron-neutron cross section, σ_{nn}, is taken to be equal to the proton-proton one, σ_{pp}. Simple fits to the energy-dependent free-space total cross sections are used

for the proton-proton cross section, σ_{pp}, and the proton-neutron one, σ_{pn}.

Harmonic oscillator wave functions with a characteristic energy of $\hbar\omega = 40/A^{1/3}$ MeV are used for the projectile states. The single-particle energy levels are obtained from a spherical Nilsson scheme with the same characteristic energy but including spin-orbit splitting and an $\boldsymbol{l} \cdot \boldsymbol{l}$ shift.

Abrasion matrix elements were calculated for various nuclei using the complete radial and angular wave functions for each state and, again, using just the radial wave functions of each level. A comparison of the resulting primary cross sections and energy distributions revealed negligible differences. In the results presented here, each abrasion matrix element is calculated with just the radial wave function of a level and is then used for all of the states of that level. This approximation can substantially reduce the execution time of the combinatorial calculation of primary yields and energy distributions. It does so by reducing the sum over the combinations of occupied states in each partially filled level to a simple binomial factor.

As the number of abraded nucleons increases, combinatorial calculations of the primary yields and the energy distributions of Eq. (34) quickly become unfeasible. In such cases, saddle-point approximations can be used to obtain quite good estimates of the yields and energy distributions. These approximations are described in detail in Appendices C and D. A comparison shows the approximate yields to be within 10% of the combinatorial ones when two particles are abraded and within 5% when three are abraded. In the calculations, the saddle-point approximations to the primary yields and energy distributions are used whenever the number of abraded protons or neutrons exceeds six and the excitation energy exceeds 20 MeV. The exact combinatorial yields are used at lower excitation energy or when fewer than six protons and neutrons have been abraded.

In Fig. 1, the primary fragment cross section of the microscopic model, for 600 MeV/nucleon ^{40}Ar incident on ^{12}C, is compared to that of the geometrical model of Ref. [2]. The cross section of the microscopic model follows fairly closely the trend of the geometrical one except at large values of the primary fragment mass. Due to the diffuse surface of the nuclei in the microscopic model, it places the abrasion of a few nucleons at larger values of the impact parameter than the sharp-surfaced geometrical model does. The resulting cross sections are thus larger. As the overlap of the two nuclei increases, the surface contribution becomes less important and the microscopic and geometric cross sections tend to coincide.

The average excitation energy of the microscopic model is compared to that of the geometrical model in Fig. 2, again for 600 MeV/nucleon ^{40}Ar incident on ^{12}C. The average value of the excitation energy in the microscopic model lies well above the collective excitation estimate of the geometrical model. The width of the energy distribution of the microscopic model is also shown in the figure. The geometrical model predicts a unique excitation energy for the fragments of a given mass and charge. In contrast, the microscopic one predicts a wide range of excitation energies for these same fragments. It is important to take this range of energies into account when calculating their decay.

The emission of gammas, neutrons, protons, and alpha particles is taken into account in the statistical decay of the ablation stage. The giant dipole resonance is assumed to dominate the γ emission. Cross sections for particle emission are obtained from global fits to reaction cross sections. The calculations use low-energy constant-temperature level densities matched to higher-energy Fermi-gas ones with level density parameters of $a \sim A/7 - A/8$ MeV^{-1}, pairing shifts of $12/\sqrt{A}$ MeV, and experimental ground state masses. The calculations are performed using the Weisskopf-Ewing evaporation formalism in which angular momentum conservation is neglected [26]. Since a simple extension of the combinatorial calculations shows the average angular momentum

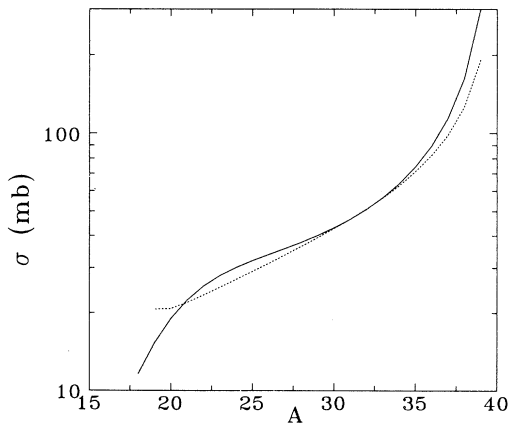

FIG. 1. Primary fragment production cross sections of the reaction ^{40}Ar + ^{12}C are shown for the microscopic model (solid line) and the geometrical model of Ref. [2] (dotted line).

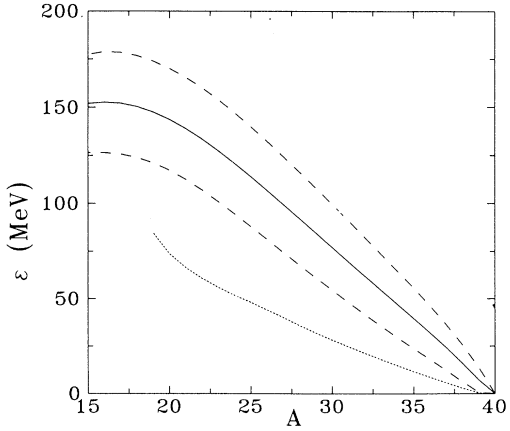

FIG. 2. Average excitation energy of the primary fragments of the reaction ^{40}Ar + ^{12}C is shown for the microscopic model (solid line) and the geometrical model of Ref. [2] (dotted line). The width of the excitation energy distribution of the microscopic model is denoted by the dashed lines.

of the fragments to be small, at least for light nuclei, this approximation seems reasonable.

B. Comparison with experiment

Model calculations are compared, in Fig. 3, to the secondary elemental and isotopic yields of Ref. [7] for the reaction ^{24}Mg + ^{12}C at E_{lab}= 600 MeV/nucleon. The experimental cross sections are fairly well described by the calculations, with the exception of the yields of neon and fluorine. The calculation overestimates the elemental yield of neon and underestimates that of fluorine, which has one less unit of charge. This suggests that the real neon fragments have more excitation energy than the calculation attributes to them and, thereby, emit a proton to form fluorine residues more frequently than predicted by the calculation. However, the calculated fluorine yields that disagree most with the data are at least two mass units lighter than the discrepant neon isotopes. The formation of a fluorine isotope by decay of the neon ones would thus require the emission of at least a proton and a neutron, which would require even more excitation energy. As the other isotopic yields are fairly well described by the calculation, the disagreement between calculation and experiment could instead be due to details of their nuclear structure.

In Fig. 4, the secondary elemental and isotopic yields of Ref. [7] for the reaction ^{40}Ar + ^{12}C at E_{lab}= 600 MeV/nucleon are compared to the model calculations. In this case, the overall agreement between the calculation and the data is quite good. A systematic discrepancy does appear in the yields of the heaviest isotope of chlorine, sulphur, and phosphorus, which are overestimated by the calculation. As the production cross sections of these isotopes are almost completely determined by the abrasion cross sections to their ground states (the formation of any of these isotopes in an excited states almost always results in decay), we can conclude that the ground state production is overestimated in the abrasion stage. This is an indication that processes more complicated than the sudden abrasion one will need to be taken into account to describe these cross sections.

Increasing the mass of the projectile accentuates the systematic discrepancy between the experimental data and the model results. This can be clearly seen in Fig. 5, where the secondary elemental and isotopic yields, again of Ref. [7], for the reaction ^{56}Fe + ^{12}C at E_{lab}= 600 MeV/nucleon are compared to the model calculations. Although the calculation describes the general trend of the data quite well, it overestimates the yields of the heavier isotopes of each element by factors of 2–5. A slight tendency to overestimate the yields of the lighter isotopes is also noticeable here. The excessive heavy isotope yields again suggest that processes other than the abrasion one play a role in the fragmentation.

The model calculations clearly disagree with fragmentation data for heavy projectiles, as exemplified in Fig. 6, which compares calculated isotopic yields of the reaction ^{197}Au + ^{27}Al at E_{lab}=1 GeV/nucleon to the experimental ones of Ref. [12]. The calculation greatly overestimates the yields of neutron-rich isotopes and underestimates the yields of neutron-deficient ones. The calculated secondary yields lie between the calculated primary yields from which they originated and the experimentally observed yields. This is an indication that, at least in this case, insufficient excitation energy is provided to the primary fragments in the model calculations. Indeed, the authors of Ref. [12], using the statistical abrasion model of Gaimard and Schmidt [14],

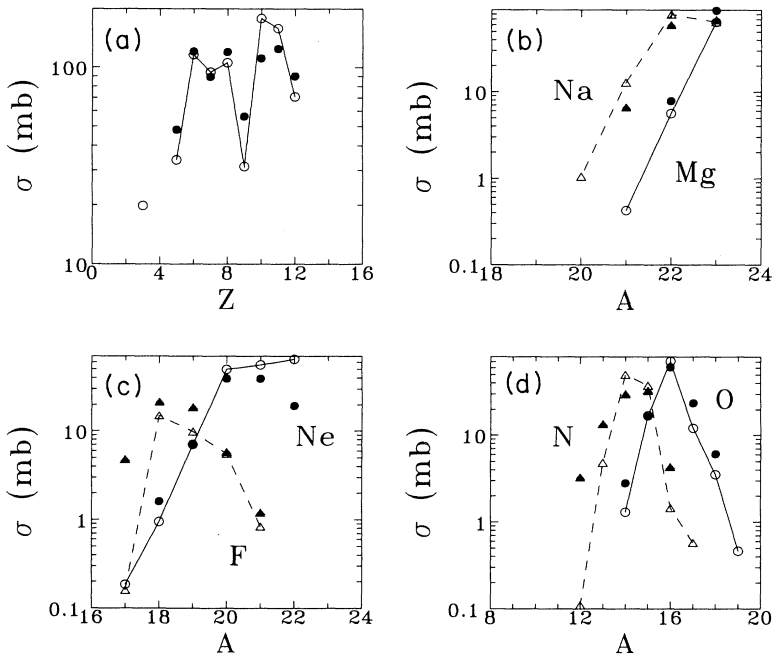

FIG. 3. Calculated secondary yields in the reaction ^{24}Mg + ^{12}C at E_{lab}=600 MeV/nucleon are shown as connected open symbols for (a) elemental yields and for the isotopes of (b) magnesium and sodium, (c) neon and fluorine, and (d) nitrogen and oxygen. The data of Ref. [7] are shown as solid symbols. The experimental errors are smaller than the size of the symbols.

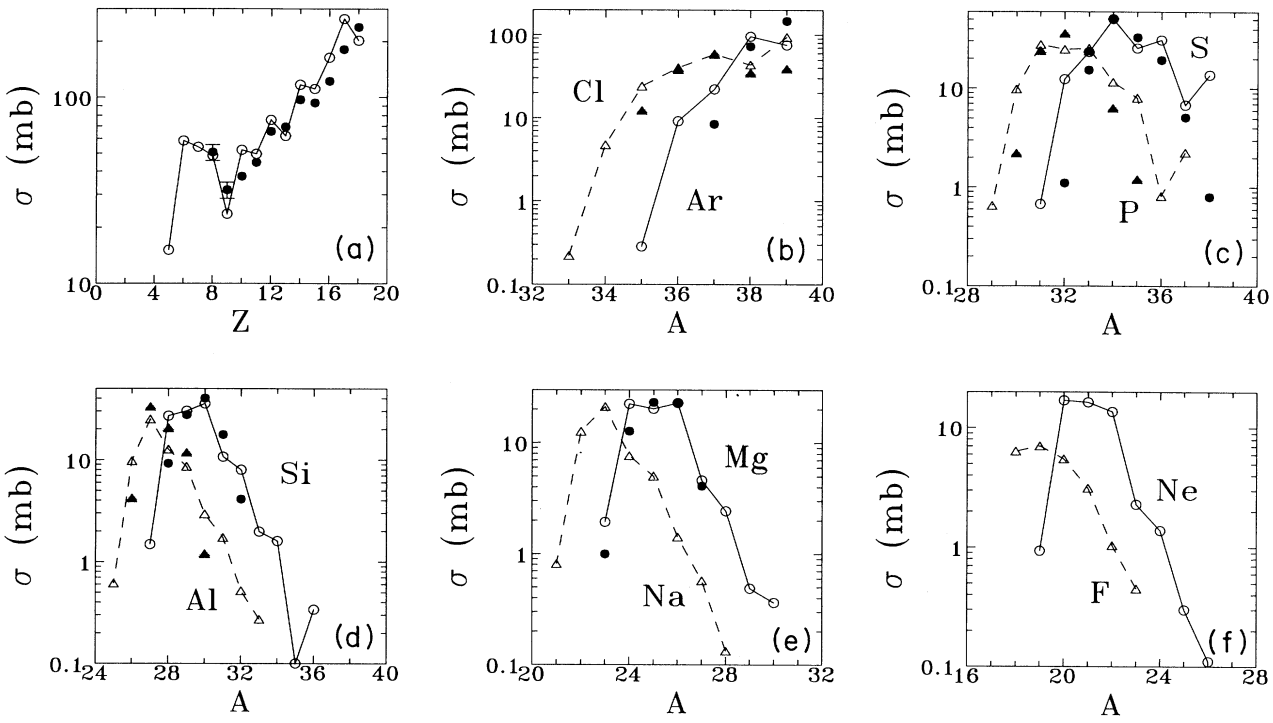

FIG. 4. Calculated secondary yields in the reaction $^{40}Ar + {}^{12}C$ at E_{lab}=600 MeV/nucleon are shown as connected open symbols for (a) elemental yields and for the isotopes of (b) argon and chlorine, (c) sulfur and phosphorus, (d) silicon and aluminum, (e) magnesium and sodium, and (f) neon and fluorine. The data of Ref. [7] are shown as solid symbols. The experimental errors are shown only where they exceed the size of the symbols.

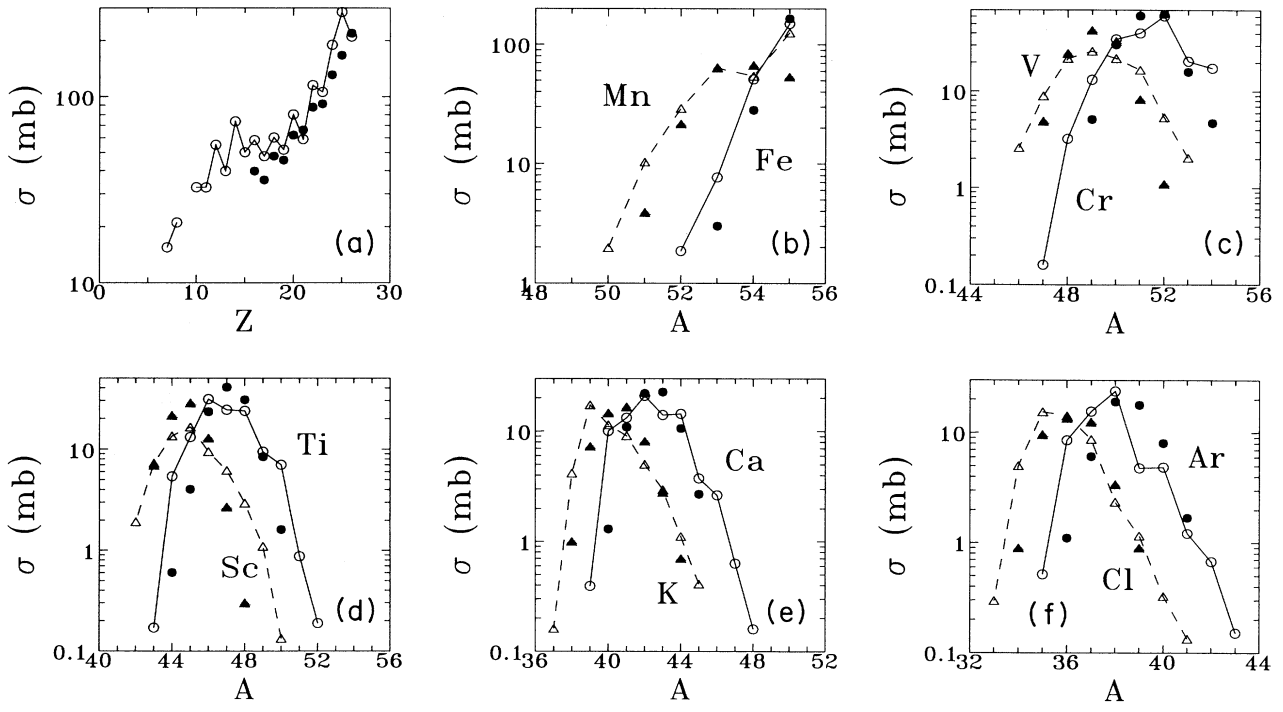

FIG. 5. Calculated secondary yields in the reaction $^{56}Fe + {}^{12}C$ at E_{lab}=600 MeV/nucleon are shown as connected open symbols for (a) elemental yields and for the isotopes of (b) iron and manganese, (c) chromium and vanadium, (d) titanium and scandium, (e) calcium and phosphorus, and (f) argon and chlorine. The data of Ref. [7] are shown as solid symbols. The experimental errors are smaller than the size of the symbols.

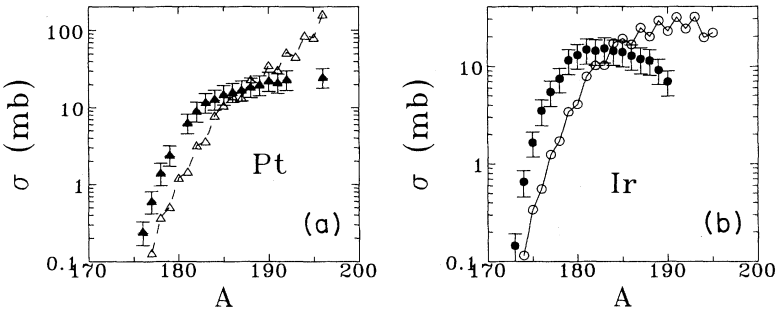

FIG. 6. Calculated secondary yields in the reaction ^{197}Au + ^{27}Al at $E_{\rm lab}$=1 GeV/nucleon are shown as connected open symbols for the isotopes of platinum and iridium. The data of Ref. [12] are shown as solid symbols with error bars.

were able to adjust their calculation to the experimental data by doubling the average excitation energy provided to the primary fragments. A similar modification of the microscopic model (made by doubling the energies of the single-particle states) does not prove as successful, since it does not modify the ground-state–to–ground-state fragmentation yields.

In summary, comparison of the microscopic abrasion-ablation model to the experimental data shows good overall agreement for light nuclei. Small discrepancies between the experimental and calculated yields of the heaviest fragments become larger as the mass of the projectile increases. The calculated yields from heavy projectiles show discrepancies with the experimental data for both light and heavy fragments. Insufficient excitation energy of the calculated primary fragment distribution seems to be responsible, at least in part, for these discrepancies. It thus appears that the microscopic model still underestimates the average excitation energy of the abraded fragments, although it does so to a much lesser degree than does the geometric model.

C. Discussion

In this section, we discuss the role played by the secondary collisions of abraded nucleons with the projectile fragment in explaining the general agreement of the model with the data for light projectiles and its disagreement for heavy ones. The projectile provides an ever bigger target for such interactions as its mass increases, thus increasing their probability and importance. Illustrative calculations presented in the following corroborate this trend.

To study the relative importance of primary and secondary nucleon-nucleon collisions, we use the Boltzmann-Uehling-Uhlenbeck (BUU) equation, thereby approximating the time evolution of the nuclear collision in terms of the time evolution of the corresponding one-particle density. Solutions to the BUU equation were obtained using the test-particle method [20] as implemented in the code by Bauer [28].

The BUU code was modified to calculate the average numbers of various types of nucleon-nucleon collisions occurring during the reaction. The test-particle method of solving the BUU equation lends itself easily to the calculation of collision numbers. It simulates a large number of similar reactions at the same time, using their averages to determine average quantities, such as the mean field and Pauli blocking factors, but confining the individual nucleon-nucleon collisions within each of the similar reactions. The calculation of average numbers of collisions then reduces to a simple classification and counting of the collisions that occur. As the collisions must be counted individually for each test particle, it is also an easy matter to extract information about the average number of nucleons that participate in each type of collision.

We group the collisions into three types: primary, secondary, and tertiary ones. We call a collision between a projectile and a target nucleon a primary one. We take as secondary collisions those between either two projectile nucleons or two target nucleons, in which at least one of the pair has already undergone a primary collision. We call all other collisions tertiary ones. For a tertiary collision to occur in the simulations, at least one of the nucleons must first participate in at least one primary and one secondary collision. (It is the *other* nucleon in the secondary collision that induces the tertiary one.) Tertiary collisions thus tend to be less energetic than the primary and secondary ones and are, thus, of less importance to the abrasion process. They can still play an important role in the equilibration of the excitation energy, however.

The Glauber approximation to the abrasion cross sections takes into account the interaction between the projectile and the target nucleons. We would thus expect it to approximate well the average number of primary collisions and the average number of nucleons abraded in these collisions. Within the approximation, the average number of abraded nucleons, $A_{\rm abr}$, can be written as the sum of the probabilities of being abraded of each of the initially occupied orbitals,

$$A_{\rm abr}(\mathbf{b}) = \sum_{j\in\mathcal{O}_0} \left(1 - |\overline{Q}_j(\mathbf{b})|^2\right) . \tag{38}$$

The average number of collisions plays no explicit role in our development of the Glauber approximation. However, we can use it to estimate the average collision number for each projectile orbital with the following intuitively reasonable expression,

$$N_j(\mathbf{b}) = \int dz\, d^2s\, |o_j(z,\mathbf{s})|^2 \sigma_{NN} \int dz'\, \rho^T(z', \mathbf{b}-\mathbf{s}) , \tag{39}$$

where ρ^T is the total target nucleon density. That is,

we estimate the number of collisions as the average, over each orbital, of the mean number of target nucleons encountered [29]. The total number of collisions, $N_{\rm coll}$, is then the sum over all orbitals of their average numbers of collisions,

$$N_{\rm coll}(\mathbf{b}) = \int dz\, d^2s\, \rho^P(z,\mathbf{s})\sigma_{NN} \int dz'\, \rho^T(z',\mathbf{b}-\mathbf{s})\ , \tag{40}$$

with ρ^P being the total nucleon density of the projectile. These expressions are easily generalized to take into account the difference between neutrons and protons. The generalized expressions were used in the calculations.

We compare, in Figs. 7 and 8, the average number of collisions, $N_{\rm coll}(b)$, and the average number of struck nucleons, $A_{\rm abr}(b)$, obtained from a Glauber calculation, with those obtained from the solution of the BUU equation. The calculations shown were performed for 300 MeV/nucleon ^{16}O incident on ^{208}Pb. In Fig. 7, we show the average numbers for the ^{16}O projectile. We display the same quantities for the ^{208}Pb target in Fig. 8.

In Fig. 7(a), we show the average numbers of various types of projectile collisions as a function of the impact parameter. The number of primary collisions in the BUU calculation (solid line) is about the same as the collision number obtained from the Glauber calculation (dotted line). Both are much greater than the average number of secondary projectile collisions (long dashed line). By comparing these numbers to the total number of projectile collisions (short-dashed line), we conclude that the tertiary collisions are even fewer in number than the secondary ones. This suggests that the few nucleons that do participate in secondary collisions leave the projectile before interacting again. The projectile portion of the reaction is thus clearly dominated by the primary collisions with the target.

The average numbers of struck projectile nucleons, shown in Fig. 7(b), have characteristics similar to those seen in the collision numbers. The number of nucleons

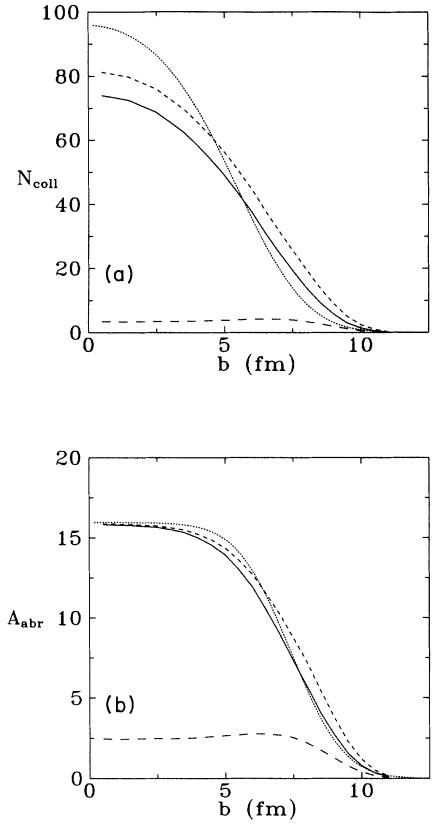

FIG. 7. The average number of collisions (a) and the average number of struck nucleons (b) as a function of the impact parameter, for the ^{16}O projectile in a collision of 300 MeV/nucleon ^{16}O incident on ^{208}Pb. The primary collisions of the BUU calculation are represented by the solid line while the dotted line represents the results of the Glauber calculation. The secondary projectile collisions are represented by the long-dashed line while the short-dashed one gives the total number of projectile collisions in the BUU calculation.

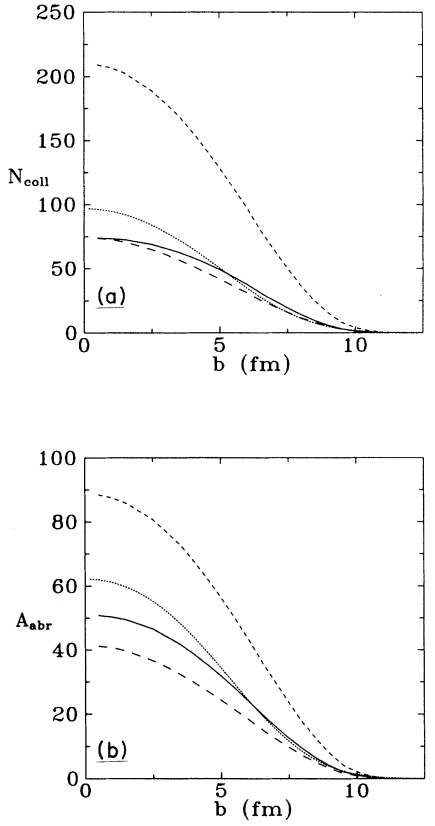

FIG. 8. The average number of collisions (a) and the average number of struck nucleons (b) as a function of the impact parameter, for the ^{208}Pb target in a collision of 300 MeV/nucleon ^{16}O incident on ^{208}Pb. The primary collisions of the BUU calculation are represented by the solid line while the dotted line represents the results of the Glauber calculation. The secondary target collisions are represented by the long-dashed line while the short-dashed one gives the total number of target collisions in the BUU calculation.

struck in primary collisions in the BUU calculation (solid line) is almost the same as that in the Glauber calculation (dotted line). Both saturate at a value of 16 at an impact parameter of about 5 fm, signifying complete abrasion of the projectile for smaller values of the impact parameter.

The number of secondary projectile nucleons saturates at a smaller value of 2.5 to 3 but at a larger impact parameter of about 7 fm. This value of the impact parameter corresponds to an overlap of about half of the oxygen nucleus with the lead one, implying the abrasion of about eight nucleons. The prescription for final-state interactions of Refs. [3,6] would estimate that an average of four of these (half of the eight) will collide with another projectile nucleon before escaping. The number obtained from the BUU calculation is slightly smaller, suggesting that at most about 35% of the primary nucleons in the oxygen projectile go on to collide with another projectile nucleon.

The number of secondary projectile nucleons does not drop back to zero as the impact parameter decreases below 7 fm and the overlap increases. This is a result of the definitions of the collision types, which permit nucleons to undergo a primary collision after having undergone a secondary one. For the same reason, the total number of struck projectile nucleons need not be the sum of the three types.

Now, let us turn our attention to the average numbers of collisions of the ^{208}Pb target nucleus, as displayed in Fig. 8(a). As expected, the number of primary collisions in the BUU calculation (solid line) is about the same as the Glauber one (dotted line). By definition, they are identical to those of the projectile in Fig. 7(a). However, the number of secondary target collisons is large and of the same order of magnitude as the primary ones. A comparison of the two to the total number of collisions reveals that the number of tertiary collisions is also sizeable, becoming even larger than the number of secondary ones for small values of the impact parameter. Thus, from the point of view of the target, the reaction looks very different than it does to the projectile. It looks very little like the fast abrasion process that we had hoped to model using the Glauber approximation.

The average numbers of struck target nucleons, shown in Fig. 8(b), corroborates this conclusion. The number of primary target nucleons (solid line) and the number from the Glauber calculation (dotted line) are again very similar. Note that, although the number of primary collisions is necessarily the same for the projectile and the target, the number of nucleons involved can be different for the two. Indeed, the number of target nucleons undergoing primary collisions is much larger than the number of projectile ones and does not saturate at low impact parameter. At complete overlap—at an impact parameter of about 5 fm—the number of primary target nucleons is about 40. At lower values of the imapct parameter, it increases even more. However, the values there should not be taken too seriously. For values of the impact parameter below about 4 fm, the projectile nucleons undergo enough collisions to be stopped in the target. This is the principal reason for the consistent difference between the primary numbers and the numbers obtained from the Glauber calculation at low values of the impact parameter.

As can be seen in Fig. 8(b), the number of secondary target nucleons is about 80% of the primary one, a fraction larger than the 50% estimate of Refs. [3,6]. The BUU calculation thus suggests that a larger and larger fraction of the primary nucleons participate in secondary collisions as the mass of the nucleus increases. Such a trend seems quite reasonable. As the mass of the nucleus increases, it provides an ever bigger target for such collisions, thereby increasing their probability.

We note that the total number of target nucleons involved in collisions is almost equal to the sum of the primary and secondary ones for values of the impact parameter larger than about 4 or 5 fm (where stopping does not occur). In this region, almost all tertiary target collisions involve secondary nucleons or target nucleons that later undergo primary or secondary collisions.

In summary, we conclude, from the comparisons with the BUU simulations, that the Glauber calculation does indeed approximate well the primary collisions between the projectile and target nucleons (at least when the nucleons are not stopped). It obviously cannot describe the secondary and tertiary collisions, as it does not take them into account. We have seen that the role played by tertiary collisons seems to be a minor one and that they can probably be neglected. We are thus left with the secondary collisions to responsiblize for the discrepancies between the Glauber calculation and the experimental data.

In light nuclei, secondary collisions are a small fraction of the total number for most values of the impact parameter. Their effect on most cross sections is small. This is not the case at extremely peripheral values of the impact parameter, where they are responsible for greatly reducing the cross sections for few-nucleon removal. As was remarked in the section comparing the model calculations to the experimental data, the latter cross sections result primarily from abrasion directly to the fragment ground state. From the lack of tertiary collisions in light nuclei, we conclude that the secondary collisions reduce these yields by knocking out more nucleons. (If the secondary collisions were to deposit energy in the fragment, we would expect it to appear in the form of subsequent tertiary collisions.)

In heavy nuclei, the situation appears more complicated at first glance. A large fraction of the primary nucleons undergo secondary collisions at all values of the impact parameter. Their effects are visible in all cross sections. A substantial fraction of tertiary collisions is also observed, suggesting that some equilibration in energy occurs. Yet, as noted above, the net number of tertiary nucleons is almost zero for impact parameters at which stopping does not occur. This suggests that there is no net deposition of energy there, as the tertiary nucleons later undergo primary or secondary collisions and do not remain in the fragment. For impact parameters at which stopping does not occur, the principal effect of the secondary collisions in heavy fragments seems to be again the abrasion of other nucleons, rather than the deposition of energy.

The seemingly sharp division between abrasive collisions and stopped, energy depositing ones, seen in the dynamical simulation, suggests a means of extending the Glauber calculation to include more of the physics of the reaction. This would be done by including secondary collisions as abrasive ones that knock out still other nucleons. Energy deposition in the fragment would only occur if the primary nucleon were to be stopped. However, before such an either/or approximation is implemented, its validity should be studied in further dynamical simulations. The contribution to the excitation energy of pion absorption following delta decay should also be verified. Work on these subjects is in progress.

IV. CONCLUSIONS

A microscopic abrasion-ablation model is developed which approximates primary fragment cross sections using the Glauber interaction probabilities of the individual nucleon orbitals. It yields primary cross sections similar to those of the geometrical model of Ref. [2]. It estimates the excitation energy distribution of the primary fragments using the density of hole states left by the abraded nucleons. It predicts the production of fragments with a wide range of excitation energies, the average of which is two to three times greater than the energy obtained in the geometrical model. Calculations confirm the general agreement with light-ion fragmentation data that was seen in simpler models using similar approximations to the excitation energy distribution [14,16]. This agreement deteriorates with increasing mass of the projectile, due to the increasing importance of secondary collisions of the abraded nucleons with the rest of the projectile. Dynamical simulations suggest that a viable model might be constructed by extending the Glauber abrasion calculation to include the effects of abrasion due to the secondary collisions. Work in this direction is being contemplated.

ACKNOWLEDGMENTS

The author wishes to thank W. Bauer for the use of his BUU code. He also wishes to thank W. Bauer, G. F. Bertsch, C. A. Bertulani, P. Danielewicz, M. Fauerbach, E. Hanelt, D. J. Morrissey, and V. Zelevinsky for discussions during the course of this work. The author acknowledges partial support from the Fundação de Amparo do Estado de São Paulo (FAPESP–Brazil) and from the U.S. National Science Foundation under Grant No. PHY-9017077.

APPENDIX A: A PROPERTY OF ANTISYMMETRIZED PRODUCTS

Here we demonstrate the validity of a general property of antisymmetrized products of the one-body matrix elements, $Q^\dagger_{jk}$ and Q_{kl}. We show that

$$\frac{1}{N!}\sum_{p,p'}(-1)^{p+p'}\prod_{j=1}^{N}\left(\sum_{k=1}^{M}Q^\dagger_{p'(j)k}Q_{kp(j)}\right)=\begin{cases}0, & M<N,\\ \displaystyle\sum_{\{k_1,\ldots,k_N\}}\sum_{p,p'}(-1)^{p+p'}\prod_{j=1}^{N}Q^\dagger_{p'(j)k_j}Q_{k_jp(j)}, & M\geq N,\end{cases}\tag{A1}$$

where, on the right-hand-side expression, we mean by $\sum_{\{k_1,\ldots,k_N\}}$ the sum over all possible N element subsets of the states $k_1, k_2, \ldots, k_M$. The p and p' sums are sums over the N elements of the set $\mathcal{M}_0$.

Let us first look at the case in which $M < N$. Since there are N terms in the product on the left-hand side, at least one of the k indices must appear in two or more of the terms when $M < N$. We can write a typical term as

$$Q^\dagger_{p'(i)k}Q_{kp(i)}Q^\dagger_{p'(j)k}Q_{kp(j)}\prod_{l}^{N-2}Q^\dagger_{p'(l)k_l}Q_{k_lp(l)}.$$

The term associated with the permutation $p'p'_{ij}$ that exchanges i and j before applying p' will be identical to the term shown but of opposite sign. The two will thus cancel. The same argument can be used to show that any term in which one of the k indices appears twice will be cancelled by an identical term of opposite sign. When $M < N$, the entire expression must then vanish.

When $M = N$, we can expand the product on the left-hand side into N^N summands, each containing a product of N terms. All but $N!$ of these summands contain at least one repeated k index and thus vanish. Each of the surviving $N!$ summands can be transformed to a "standard" one through the choice an appropriate permutation. (Remember that each of the summands must still be summed over all permutations. The choice of a standard one merely "rotates" the representation of the permutation sum but does not change its value.) Summing over the $N!$ repetitions of the standard summand yields the right-hand side expression.

Finally, if we make the same expansion of the left-hand-side when $M > N$, we find that the same arguments can be applied to the $N!$ surviving summands of each of the $\binom{M}{N}$ N-element subsets of the M states labeled by the k's, yielding the right-hand-side again.

APPENDIX B: HÜFNER, SCHÄFER, AND SCHÜRMANN

To make contact with the approximation used by Hüfner, Schäfer, and Schürmann (HSS) in Ref. [3], we return to the expression for the differential abrasion cross section, Eq. (21),

$$\overline{X}_{O\to M_F}(\mathbf{b}) = \frac{1}{A_{\rm occ}!(A_0 - A_{\rm occ})!}\sum_{p,p'}(-1)^{p+p'}\prod_{j=1}^{A_{\rm occ}}\left(\sum_{m\in{\rm occ}}\overline{Q}^{\dagger}_{p'(j)\,m}\overline{Q}_{mp(j)}\right) \times \prod_{j=A_{\rm occ}+1}^{A_0}\left(\delta_{p'(j)\,p(j)} - \sum_{m\in{\rm vac}}\overline{Q}^{\dagger}_{p'(j)\,m}\overline{Q}_{mp(j)}\right). \tag{21}$$

Integrating this over impact parameter and summing over the $A_{\rm occ}$-element subsets of $\mathcal{M}_0$, we obtain an expression for the *inclusive* cross section that HSS proposed to calculate. We have

$$\sigma_{A_{\rm occ}} = \int d^2b \sum_{\{{\rm occ}|A_{\rm occ}\}}\overline{X}_{O\to M_F}(\mathbf{b}), \tag{B1}$$

where

$$\sum_{\{{\rm occ}|A_{\rm occ}\}}\overline{X}_{O\to M_F}(\mathbf{b}) = \frac{1}{A_{\rm occ}!(A_0 - A_{\rm occ})!}\sum_{p,p'}(-1)^{p+p'}\prod_{j=1}^{A_{\rm occ}}\left(\sum_{m\in\mathcal{M}_0}\overline{Q}^{\dagger}_{p'(j)\,m}\overline{Q}_{mp(j)}\right) \times \prod_{j=A_{\rm occ}+1}^{A_0}\left(\delta_{p'(j)\,p(j)} - \sum_{m\in\mathcal{M}_0}\overline{Q}^{\dagger}_{p'(j)\,m}\overline{Q}_{mp(j)}\right). \tag{B2}$$

Note that the sums over single-particle final states in the last expression run over all states in $\mathcal{M}_0$.

HSS assumed that the number of states in $\mathcal{M}_0$ was sufficient for the sum to be well approximated using closure. They also assumed the resulting expression to be diagonal, taking

$$\sum_{m\in\mathcal{M}_0}\overline{Q}^{\dagger}_{p'(j)\,m}\overline{Q}_{mp(j)} \approx \delta_{p'(j)\,p(j)}P_{p(j)}(\mathbf{b}), \tag{B3}$$

where

$$P_j(\mathbf{b}) = \int dz d^2s\; o^{\dagger}_j(z,\mathbf{s})\left|\exp\left[-i\frac{m}{\hbar^2 k}\int_{-\infty}^{\infty}dz\,U_T^{\rm opt}(z,\mathbf{b}-\mathbf{s})\right]\right|^2 o_j(z,\mathbf{s}). \tag{B4}$$

When substituted in the expression for $\sum_{\{{\rm occ}|A_{\rm occ}\}}\overline{X}_{O\to M_F}$, the latter can be simplified to

$$\sum_{\{{\rm occ}|A_{\rm occ}\}}\overline{X}_{O\to M_F}(\mathbf{b}) = \frac{1}{A_{\rm occ}!(A_0 - A_{\rm occ})!}\sum_{p}\prod_{j=1}^{A_{\rm occ}}P_{p(j)}(\mathbf{b})\prod_{j=A_{\rm occ}+1}^{A_0}\left(1 - P_{p(j)}(\mathbf{b})\right). \tag{B5}$$

Finally, HSS took all the $P_j(\mathbf{b})$ to be equal, replacing the squared magnitude of the wave function in the probabilities by the projectile single-particle density,

$$P_j(\mathbf{b}) \approx P(\mathbf{b}) = \int dz d^2s\;\rho_P(z,\mathbf{s})\left|\exp\left[-i\frac{m}{\hbar^2 k}\int_{-\infty}^{\infty}dz\,U_T^{\rm opt}(z,\mathbf{b}-\mathbf{s})\right]\right|^2. \tag{B6}$$

With this simplification, the expression for the cross section reduces to

$$\sigma_{A_{\rm occ}} = \binom{A_0}{A_{\rm occ}}\int d^2b\;[P(\mathbf{b})]^{A_{\rm occ}}\,[1 - P(\mathbf{b})]^{A_0 - A_{\rm occ}} \tag{B7}$$

which is their final result.

APPENDIX C: APPROXIMATING THE PRIMARY YIELDS

The abrasion calculation gives, for each impact parameter, the probability for each of the single-particle orbitals to collide (or not) with the target. The probability that a nucleon in orbital j does not collide is given by

$$p_j = |Q_j(\mathbf{b})|^2. \tag{C1}$$

The probability that it collides is then

$$q_j = 1 - p_j. \tag{C2}$$

The probability that all nucleons pass unscathed is given by

$$P_{A_0} = \prod_{j=1}^{A_0} p_j \tag{C3}$$

while the probability that all collide is given by

$$P_0 = \prod_{j=1}^{A_0} q_j. \tag{C4}$$

We can condense these, as well as the probabilities for all other numbers of nucleons to pass, in a generating function

$$\mathcal{Z} = \prod_{j=1}^{A_0} (q_j + x p_j). \tag{C5}$$

Expanding this, we find that the coefficient of $x^{A_{\rm occ}}$ is the probability that $A_{\rm occ}$ nucleons pass the target without colliding. We write

$$\mathcal{Z} = \prod_{j=1}^{A_0} (q_j + x p_j) = \sum_{A_{\rm occ}=0}^{A_0} x^{A_{\rm occ}} P_{A_{\rm occ}}. \tag{C6}$$

The probabilities P_{A_0} and P_0 are easily extracted, as are the probability that all but one nucleon pass,

$$P_{A_0-1} = P_{A_0} \sum_{j=1}^{A_0} \frac{q_j}{p_j}, \tag{C7}$$

and the probability that just one nucleon passes,

$$P_1 = P_0 \sum_{j=1}^{A_0} \frac{p_j}{q_j}. \tag{C8}$$

However, the farther we get from the two limiting cases of all or none, the more complicated this combinatorial calculation becomes.

As a first step toward approximating the probabilities, we write them as

$$P_{A_{\rm occ}} = \frac{1}{2\pi i} \int_{c-i\infty}^{c+i\infty} d\mu \prod_{j=1}^{A_0} (q_j + p_j e^{-\mu}) e^{\mu A_{\rm occ}}. \tag{C9}$$

This is an identity, as the integral in combination with the factor $e^{\mu A_{\rm occ}}$ extracts only those terms in the product which contain a factor of $x^{A_{\rm occ}} = (e^{-\mu})^{A_{\rm occ}}$.

After rewriting the integral as

$$P_{A_{\rm occ}} = \frac{1}{2\pi i} \int_{c-i\infty}^{c+i\infty} d\mu \, \exp[F(\mu) + \mu A_{\rm occ}], \tag{C10}$$

where

$$F(\mu) = \sum_{j=1}^{A_0} \ln(q_j + p_j e^{-\mu}), \tag{C11}$$

we approximate it by expanding $F(\mu) + \mu A_{\rm occ}$ through second order about its stationary point μ_0. There, we have

$$\left.\frac{dF}{d\mu}\right|_{\mu=\mu_0} + A_{\rm occ} = A_{\rm occ} - \sum_{j=1}^{A_0} \frac{p_j e^{-\mu_0}}{q_j + p_j e^{-\mu_0}} = 0. \tag{C12}$$

The second derivative is

$$\left.\frac{d^2F}{d\mu^2}\right|_{\mu=\mu_0} = \sum_{j=1}^{A_0} \frac{q_j p_j e^{-\mu_0}}{(q_j + p_j e^{-\mu_0})^2} \equiv d^2F_0. \tag{C13}$$

After rotating to the real axis, the approximation to the integral can be written as

$$P_{A_{\rm occ}} \approx \frac{1}{2\pi} \int_{-\infty}^{\infty} d\mu \, \exp[F(\mu_0) + \mu_0 A_{\rm occ} - \tfrac{1}{2} d^2F_0 (\mu - \mu_0)^2] = \frac{e^{F(\mu_0) + \mu_0 A_{\rm occ}}}{\sqrt{2\pi d^2F_0}}. \tag{C14}$$

We also want to estimate the maximum and extension in mass of the distribution of probabilities. We can do this by looking for the maximum and width of the distribution of the $P_{A_{\rm occ}}$. We neglect the effects of the term d^2F_0 and look at the dependence on $A_{\rm occ}$ of the argument of the exponential, $F(\mu_0) + \mu_0 A_{\rm occ}$. The condition for the maximum is

$$\left.\frac{dF(\mu_0)}{dA_{\rm occ}}\right|_{A_{\rm occ}=A_{\rm max}} + \mu_0 = \left(A_{\rm max} - \sum_{j=1}^{A_0} \frac{p_j e^{-\mu}}{q_j + p_j e^{-\mu}} \right) \left.\frac{d\mu_0}{dA_{\rm occ}}\right|_{A_{\rm occ}=A_{\rm max}} + \mu_0 = 0. \tag{C15}$$

As the expression in parentheses must be zero to satisfy Eq. (C12), we have for the solution

$$\mu_0 = 0 \quad \text{and} \quad A_{\rm max} = \sum_{j=1}^{A_0} p_j. \tag{C16}$$

The second derivative is

$$\left.\frac{d^2F(\mu_0)}{dA_{\rm occ}^2}\right|_{A_{\rm occ}=A_{\rm max}} = \left.\frac{d\mu_0}{dA_{\rm occ}}\right|_{\mu_0=0} = -\left(\sum_{j=1}^{A_0} p_j q_j \right)^{-1}, \tag{C17}$$

where the last equality is obtained by differentiating the equation defining μ_0, Eq. (C12), with respect to $A_{\rm occ}$. Thus the distribution in mass has its maximum at

$$A_{\rm max} = \sum_{j=1}^{A_0} p_j, \tag{C18}$$

and a width of

$$\sigma_A = \sqrt{\sum_{j=1}^{A_0} p_j q_j}. \tag{C19}$$

In the calculations, this analysis is performed independently for neutrons and protons, with the combined probability obtained as the product of the individual ones,

$$P_{Z_{\rm occ}\,N_{\rm occ}} = P_{Z_{\rm occ}}\,P_{N_{\rm occ}}. \tag{C20}$$

The distributions in charge and neutrons number have their maxima at

$$Z_{\rm max} = \sum_{j_\pi=1}^{Z_0} p_{j_\pi} \quad \text{and} \quad N_{\rm max} = \sum_{j_\nu=1}^{N_0} p_{j_\nu} \tag{C21}$$

and have widths of

$$\sigma_Z = \sqrt{\sum_{j_\pi=1}^{Z_0} p_{j_\pi} q_{j_\pi}} \quad \text{and} \quad \sigma_N = \sqrt{\sum_{j_\nu=1}^{N_0} p_{j_\nu} q_{j_\nu}}\,. \tag{C22}$$

The expressions for the maximum and width of the mass distribution, Eqs. (C18) and (C19), continue valid.

The approximate yields are used in the numerical calculations whenever the number of abraded protons or neutrons exceeds six. The exact combinatorial yields are used when fewer neutrons and protons are abraded.

APPENDIX D: APPROXIMATING THE PRIMARY FRAGMENT ENERGY DISTRIBUTION

When using approximations to the primary yields, it is convenient to also approximate their energy distributions. To do this, we extend the generating function to

$$\mathcal{Z}(\beta,\mu) = \prod_{j=1}^{A_0} (q_j e^{-\beta\epsilon_j} + p_j e^{-\mu}), \tag{D1}$$

where the ϵ_j are the energies of the single-particle states. The distribution could then, in principle, be calculated as

$$\rho_{A_{\rm occ}}(\varepsilon) = \frac{1}{(2\pi i)^2}\int_{b-i\infty}^{b+i\infty} d\beta \int_{c-i\infty}^{c+i\infty} d\mu\, \exp[F(\beta,\mu) + \mu A_{\rm occ} + \beta\varepsilon], \tag{D2}$$

with

$$F(\beta,\mu) = \sum_{j=1}^{A_0} \ln(q_j e^{-\beta\epsilon_j} + p_j e^{-\mu}). \tag{D3}$$

Instead, we perform the μ integral as in Appendix C, but now for each value of β. We find

$$\rho_{A_{\rm occ}}(\varepsilon) = \frac{1}{\sqrt{2\pi d^2 F_0}}\frac{1}{2\pi i}\int_{b-i\infty}^{b+i\infty} d\beta\, \exp\{F[\beta,\mu(\beta)] + \mu(\beta)A_{\rm occ} + \beta\varepsilon\}, \tag{D4}$$

with $\mu(\beta)$ determined by the condition

$$\left.\frac{dF}{d\mu}\right|_{\mu=\mu(\beta)} + A_{\rm occ} = A_{\rm occ} - \sum_{j=1}^{A_0} \frac{p_j e^{-\mu(\beta)}}{q_j e^{-\beta\epsilon_j} + p_j e^{-\mu(\beta)}} = 0. \tag{D5}$$

We have assumed that the second derivative, $d^2F/d\mu^2$, is a slowly varying function of β, approximated it by its value at $\beta = 0$, and removed it from the integral.

Integrating the density of states of Eq. (D4) over the excitation energy, we obtain the result of Eq. (C14)

$$P_{A_{\rm occ}} = \int \rho_{A_{\rm occ}}(\varepsilon) = \frac{e^{F(0,\mu_0)+\mu_0 A_{\rm occ}}}{\sqrt{2\pi d^2 F_0}}, \tag{D6}$$

since

$$\mu(\beta)|_{\beta=0} = \mu_0. \tag{D7}$$

We calculate the moments of the energy distribution using the identity

$$\langle \varepsilon^n \rangle = e^{-F(0,\mu_0)-\mu_0 A_{\rm occ}} \left(-\frac{d}{d\beta}\right)^n e^{F[\beta,\mu(\beta)]+\mu(\beta)A_{\rm occ}}\Big|_{\beta=0}, \tag{D8}$$

and make use of the derivatives of the condition defining $\mu(\beta)$, Eq. (D5), to evaluate the derivatives, $d^n\mu/d\beta^n$, that appear in the resulting expressions. We then require that these be the moments of an approximate distribution of the form

$$\rho_{A_{\rm occ}}(\varepsilon) = \frac{P_{A_{\rm occ}}}{\sqrt{2\pi\sigma^2}}\left(1 + \sum_{n=3}^{6} \frac{\alpha_n}{(\sqrt{2}\sigma)^n n!} H_n\left(\frac{\varepsilon-\bar{\varepsilon}}{\sqrt{2}\sigma}\right)\right) \exp\left[-\frac{(\varepsilon-\bar{\varepsilon})^2}{2\sigma^2}\right], \tag{D9}$$

where H_n denotes the Hermite polynomial of order n. A straightforward but tedious comparison of the moments of the latter distribution with those of Eq. (D8), permits the identification of the distribution's parameters as

$$\bar{\varepsilon} = -\left.\frac{d\{F[\beta,\mu(\beta)]+\mu(\beta)A_{\rm occ}\}}{d\beta}\right|_{\beta=0}, \quad \sigma^2 = \left.\frac{d^2\{F[\beta,\mu(\beta)]+\mu(\beta)A_{\rm occ}\}}{d\beta^2}\right|_{\beta=0}, \tag{D10}$$

$$\alpha_n = (-1)^n \left.\frac{d^n\{F[\beta,\mu(\beta)]+\mu(\beta)A_{\rm occ}\}}{d\beta^n}\right|_{\beta=0}, \quad n=3,4,5,$$

and (D11)

$$\alpha_6 = \left.\frac{d^6\{F[\beta,\mu(\beta)]+\mu(\beta)A_{\rm occ}\}}{d\beta^6}\right|_{\beta=0} + 10(\alpha_3)^2.$$

In practice, the quantities $\bar{\varepsilon}$, σ^2 and the α_n are calculated independently for protons and neutrons. With the exception of α_6, the corresponding values for the combined distribution are the sums of the values for the individual distributions, since these quantities are their cumulants. The value of α_6 for the combined distribution is also easily obtained by noting that it differs from the sixth-order cumulant by just the $(\alpha_3)^2$ term.

The approximate distributions are used in the numerical calculations, for the fraction of the yield above 20 MeV in excitation energy, whenever the number of abraded protons or neutrons exceeds six. The distribution of the fraction of the yield that lies below 20 MeV in excitation energy is calculated combinatorially.

[1] R. Serber, Phys. Rev. **72**, 1114 (1947).
[2] J. D. Bowman, W. J. Swiatecki, and C. F. Tsang, LBL Report No. LBL-2908, 1973 (unpublished).
[3] J. Hüfner, K. Schäfer, and B. Schürmann, Phys. Rev. C **12**, 1888 (1975).
[4] G. Gelbke, C. Olmer, M. Buenerd, D. L. Hendrie, J. Mahoney, M. C. Mermaz, and D. K. Scott, Phys. Rep. **42**, 312 (1978).
[5] D. K. Scott, in *Proceedings of the NATO Advanced Studies Institute on Theoretical Methods in Medium-Energy and Heavy-Ion Physics*, University of Wisconsin, Madison, 1978, edited by K. W. McVoy and W. A. Friedman, (Plenum, New York, 1978).
[6] L. F. Oliveira, R. Donangelo, and J. O. Rasmussen, Phys. Rev. C **19**, 826 (1979).
[7] W. R. Webber, J. C. Kish, and D. A. Schrier, Phys. Rev. C **41**, 520 (1990); **41**, 530 (1990); **41**, 547 (1990).
[8] F. Deák, A. Kiss, Z. Seres, A. Galonsky, L. Heilbronn, and H. R. Schelin, Phys. Rev. C **42**, 1029 (1990).
[9] C. Stephán, L. Tassan-Got, D. Bachelier, C. O. Barci, R. Bimbot, B. Borderie, J. L. Boyard, F. Clapier, D. Donzaud, T. Hennino, M. F. Rivet, P. Roussel, D. Bazin, C. Grunberg, D. Disdier, and B. Lott, Phys. Lett. B **262**, 6 (1991).
[10] J. Dreute, W. Heinrich, G. Rusch, and B. Wiegel, Phys. Rev. C **44**, 1057 (1991).
[11] G. A. Souliotis, D. J. Morrissey, N. A. Orr, B. M. Sherrill, and J. A. Winger, Phys. Rev. C **46**, 1383 (1992).
[12] K.-H. Schmidt, T. Brohm, H.-G. Clerc, M. Dornik, M. Fauerbach, H. Geissel, A. Grewe, E. Hanelt, A. Junghaus, A. Magel, W. Morawek, G. Münzenberg, F. Nickel, M. Pfützner, C. Scheidenberger, K. Sümmerer, D. Vieira, B. Voss, and C. Zeigler, Phys. Lett. B **300**, 313 (1993).
[13] G. Bertsch, H. Esbensen, and A. Sustich, Phys. Rev. C **42**, 758 (1990).
[14] J. J. Gaimard and K. H. Schmidt, Nucl. Phys. **A531**, 709 (1991).
[15] G. Lanzanó, A. Pagano, E. De. Filippo, R. Dayras, and R. Legrain, Z. Phys. A **343**, 429 (1992).
[16] B. V. Carlson, M. S. Hussein, and R. C. Mastroleo, Phys. Rev. C **46**, R30 (1992).
[17] F. Khan and L. W. Townsend, Phys. Rev. C **48**, R513 (1993).
[18] I. Tanihata, Treatise Heavy-Ion Sci. **8**, 443 (1989).
[19] Y. Yariv and Z. Fraenkel, Phys. Rev. C **20**, 2227 (1979).
[20] G. F. Bertsch and S. das Gupta, Phys. Rep. **160**, 189 (1988).
[21] J. Aichelin and H. Stöcker, Phys. Lett. B **176**, 14 (1986); J. Aichelin, Phys. Rep. **202**, 223 (1991).
[22] H. Feldmeier, Nucl. Phys. **A515**, 147 (1990).
[23] A. Ono, H. Horiuchi, T. Maruyama, and A. Ohnishi, Prog. Theor. Phys. **87**, 1185 (1992).
[24] R. J. Glauber, in *Lectures in Theoretical Physics*, Proceedings of the Lectures Delivered at the Summer Institute for Theoretical Physics, University of Colorado, Boulder, 1958, edited by W. E. Brittin and L. G. Dunham (Interscience Publishers, New York, 1959), Vol. 1, pp. 315–414.
[25] N. Takigawa, M. Ueda, M. Kuratani, and H. Sagawa, Phys. Lett. B **288**, 244 (1992).
[26] V. F. Weisskopf and D. H. Ewing, Phys. Rev. **57**, 472 (1940); **57**, 935 (1940).
[27] de Jager, de Vries, and de Vries, At. Data Nucl. Data Tables **14**, 479 (1974).
[28] W. Bauer, Nucl. Phys. **A471**, 604 (1987).
[29] R. J. Glauber and G. Matthiae, Nucl. Phys. **B21**, 135 (1970).